The Intricate Dynamics of the Si(3P) + OH(X2Π) Reaction

Alejandro Rivero Santamaría, Pascal Larregaray, Laurent Bonnet, Fabrice Dayou, Maurice Monnerville

The Intricate Dynamics of the Si(^{3}P)+OH($X^2\Pi$) Reaction

Alejandro Rivero Santamaría,[†] Pascal Larregaray,[‡] Laurent Bonnet,[‡] Fabrice Dayou,[¶] and Maurice Monnerville[*,†]

†*Laboratoire de Physique des Lasers, Atomes et Molécules, UMR 8523 du CNRS, Centre d'Études et de Recherches Lasers et Applications, Université Lille I, Bât. P5, 59655 Villeneuve d'Ascq Cedex, France*

‡*groupe THEO, ISM UMR5255, CNRS/Université Bordeaux, Bat A12 351 cours de la libération, 33405 Talence cedex, France*

¶*Sorbonne Université, Observatoire de Paris, Université PSL, CNRS, LERMA, F-92195 Meudon, France*

E-mail: maurice.monnerville@univ-lille.fr

Abstract

The dynamics of the Si(^{3}P)+OH(X$^2\Pi$) $\rightarrow$ SiO(X$^1\Sigma^+$,v',j')+H(^2S) reaction is investigated by means of the quasi-classical trajectory method on the electronic ground state X^2A' potential energy surface in the 10^{-2} − 1eV collision energy range. Although the reaction involves the formation of a long-lived intermediate complex, a high probability for back-dissociation to the reactants is found because of inefficient intra-vibrational redistribution of energy among the complex modes. At low collision energies, the reactive events are governed by a dynamics with mixed direct / indirect features. As the collision energy increases, the intermediate complex lifetime increases and final state distributions are found to be in reasonable agreement with statistical predictions obtained using the mean potential phase space theory, thus highlighting the indirect character of the process. These rich and puzzling dynamical features are in line with what has been previously observed for the S(^{3}P)+OH(X$^2\Pi$) reaction.

1 Introduction

The SiO molecule is often used as a tracer to detect the jets and outflows produced in interstellar regions during the formation of stars.[1–5] While SiO is almost absent in quiescent cold clouds, its abundance increases significantly in warm shocked layers of outflows associated with nascent stars. According to astrophysical models ,[5–8] the Si+OH reaction is expected to be one of the major formation processes of interstellar SiO in the gas-phase. Unfortunately, in spite of its astrochemical relevance, no experiment has been devoted to study the Si+OH reaction kinetics. Such an experiment might indeed reveal tedious to perform as the reaction involves two radical species.[9] Consequently, a series of theoretical works[10–14] have been developed recently by some of us to investigate the Si+OH reactivity. We here complement this work by a detailed study of its dynamics at the state-to-state level and compare with that of analogous reactions of OH($X^2\Pi$) with C(^3P),[15] N(^4S),[16] O(^3P),[17] and S(^3P)[18] which have been studied in the last decade owing to their their astrophysical interest. Although all four exoergic processes involve deep potential energy wells on way from reactants to products, making possible the formation of a long-lived interme-

diate complex, the reaction dynamics are significantly different. While the C+OH collision leads to a rapid direct reaction with unit reaction probability up to 1 eV collision energy, the dynamics of the processes involving N, O and S are more intricate. These collisions, indeed, involve the formation of a long-lived intermediate complex back-dissociating with a high probability due to inefficient couplings between the complex vibrational modes. Nevertheless, for reactive events, the dynamics is dominated by an indirect mechanism in the case of the N and O atoms, and the shapes of product state distributions and differential cross-sections are consistent with those predicted by statistical theories up to 0.5 eV collision energy. The process involving S is peculiar as it is governed by mixed direct/indirect mechanisms at low collision energies (< 0.1 eV), whereas the dynamics tends to proceed mainly by indirect mechanisms upon increasing the collision energy.

The first global potential energy surface (PES) for the $Si(^3P)+OH(X^2\Pi)\rightarrow SiO(X^1\Sigma^+)+H(^2S)$ reaction has been reported recently.[10] The reaction is exoergic by 3.6 eV and proceeds adiabatically through the ground X^2A' electronic state. The X^2A' PES is barrierless, except for the approach of the reactants at nearly linear Si-HO geometry, for which a 0.2 eV potential energy barrier shows up. The PES supports two deep energy wells along the reaction path, corresponding to the stable SiOH and HSiO isomers, with depths of 5.1 eV and 4.7 eV, respectively, relative to the Si+OH dissociation limit.

In previous works[11–14] reaction probabilities, integral cross sections, state-selected and thermal rate constants were determined by means of the Quasi-Classical Trajectory (QCT) method,[11,13] time-dependent wave-packet (TDWP) approach[11,12] and mean potential phase space theory (MPPST).[11,14] Reaction probabilities were found remarkably low (< 0.5) for such a barrierless exoergic reaction. This feature, which has been observed for analogous systems,[16–18] was attributed to backdissociation of the SiOH intermediate complex due to inefficient Intra Vibrational Redistribution (IVR) between the internal modes of SiOH, thus hindering the SiOH→SiO+H and SiOH→HSiO→SiO+H reaction pathways.[12] Besides, at low collision energies, and for $J = 0$ total angular momentum, dense resonance structures associated with long-lived quasi-bound states supported by the SiOH and HSiO wells of the PES have been observed in TDWP calculations.[11,12]

The present work reports a detailed study of the state-to-state reaction dynamics of the title reaction using the QCT method for collision energies ranging from 10^{-2} to 1 eV. Possible reaction pathways, complex formation dynamics, reaction probabilities and product state distributions are under scrutiny. Comparison with MPPST results[11,14] allows to discuss the possible statistical features of the reaction dynamics. Most of the results reported in this work assume OH in its ground vibrational and rotational state, OH($v = 0, j = 0$). Nevertheless, we also discuss the effect of the initial rotational excitation on product state distributions.

2 Methodology

The Quasi-Classical Trajectory (QCT) method used in this work has been detailed elsewhere.[11–13] Briefly, batches of 10^5 trajectories are run for each collision energy E_c and ro-vibrational state of OH, following a standard Monte Carlo sampling[19] of the initial conditions. The initial atom-diatom separation is set to 40 a_0. The set of Hamilton equations is integrated using the step adaptive Runge-Kutta algorithm[20] with a relative precision of 10^{-8} for distances and momenta, ensuring the conservation of the total energy and total angular momentum with an average error of 10^{-9} eV and 10^{-10} $\hbar$, respectively. Trajectories are stopped when the separation between final fragments is greater than 20 a_0 and their recoil energy varies by less than 10^{-7} eV between two consecutive time steps. The product rotational quantum number j' specifying the SiO rotational state is assigned by first applying the semi-classical quantization $|\mathbf{j}'|^2 = \hbar^2 j'(j'+1)$ of the classical rotational angular momentum. The real j' value is then rounded to the nearest interger (Histogrammatic Binning, HB).[19] The vibrational quantum number v' of SiO is computed by the semi-classical quantization of the vibrational action integral[21]:

$$\oint p'_r \, dq' = \left(v' + \frac{1}{2}\right) 2\pi\hbar, \tag{1}$$

where $p'_r = \mu_{\mathrm{SiO}}\dot{q}'$ is the conjugate momentum of q', the SiO bond length. The real v' value is then rounded to its nearest integer. The HB method is here employed to assign both the rotational

and vibrational quantum numbers. The alternative Gaussian Binning method[22–24] was also implemented and led to similar results because of the significant number of product states available.

Mean Potential Phase Space Theory[25,26] is also applied to the title reaction in order to assess the possible statistical character of this complex-forming process. The approach relies on the assumption of a statistical (microcanonical) distribution of the internal states of the intermediate complex in a period of time much smaller than the average time for dissociation. In such a case, dynamical observables can be predicted from the calculation of individual capture probabilities from the reactant and product states. The MPPST method is a variant of Phase Space Theory[25,27,28] for which, instead of approximating the potential energies of interaction between separated fragments by their isotropic long-range contributions, the latter are replaced by the accurate potential energies averaged over Jacobi angles. This correction allows to implicitly accounts for weak anisotropies in the asymptotic channels. The integral, differential cross sections and rate constants obtained from MPPST turn out to be in very satisfying agreement with the benchmark predictions of time-independent and time-dependent statistical quantum methods[17,25,26,29–32] for barrier-less processes. In the present implementation, the average potentials, $\overline{V}(R)$, in the reactant and product channels, are computed from the *ab initio* PES, $V(R, r, \theta)$,[10] as:

$$\overline{V}(R) = \frac{1}{2} \int_0^\pi d\theta \sin\theta \; V(R, r_{\rm eq}, \theta), \tag{2}$$

where (R, r, θ) are reactant or product Jacobi coordinates, and $r_{\rm eq}$ is the equilibrium geometry of the reactant or product diatomic molecule. By averaging the PES over OH orientations, the electrostatic contributions to long-range interactions are almost cancelled (dipole/quadrupole and quadrupole/quadrupole interactions in the reactant channel,[33] varying as $1/R^4$ and $1/R^5$, respectively). The average potentials are then approximated by an effective contribution of dispersion and induction interactions of the form :

$$\overline{V}(R) = -\frac{C_6}{R^6} \tag{3}$$

where C_6 (Si + OH)= 360 eV Å^6 and C_6 (SiO + H)= 86 eV Å^6 are obtained by fitting the average potential to the form of Eq. 3 in the reactant and product channels, respectively. Furthermore, the reactant and product diatoms are treated as rigid rotor anharmonic oscillators.[34]

3 Results and Discussion

3.1 Reaction mechanisms

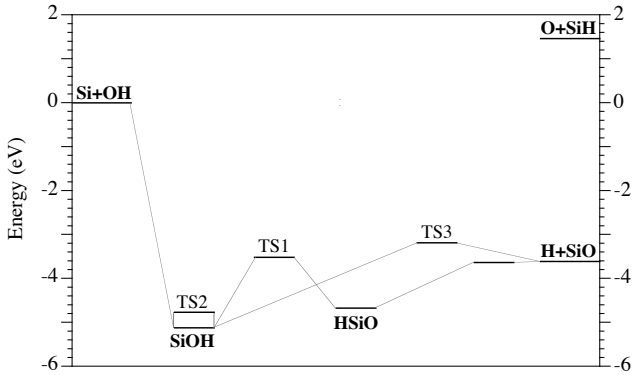

Figure 1: Energetic diagram of relevant stationary points of the X^2A' PES for the SiOH system. The energies are given relative to the Si+OH(r_{eq}) dissociation limit. TS is used to label the energy barriers associated with transition states.

The PES for the X^2A' ground electronic state of the title reaction, which has been thoroughly examined previously,[10] presents two deep energy wells corresponding to the bent SiOH and HSiO stable isomers. The minimum energy path, Si+OH→ SiOH→TS1→HSiO→H+SiO, is illustrated in Fig. 1.

The topology of the PES favors the attraction of the Si atom from the O side of the OH diatom, and only the SiOH well is accessible from the reactants. Once SiOH is formed, it might invert to the symmetric SiOH isomer (overcoming an inversion energy barrier TS2 of 0.3 eV), isomerize towards HSiO (through the energy barrier TS1 of 1.6 eV) or directly dissociate to the SiO+H products (through the energy barrier TS3 of 1.9 eV). All the transition states and minima are far below the energy of the reactants, and, therefore, all these reaction paths are energetically available at vanishing collision energies.

In order to characterize the contribution of the SiOH and HSiO isomers to the overall dynamics, the reactive trajectories have been discriminated according to the PES regions probed by the nuclei during the course of the reaction. Whereas the energetics and structural properties of the SiOH/HSiO equilibrium geometries are well defined (see Table III in Ref.[10]), there is no rigorous definition of the intermediates complexes of a reaction, especially within a three-dimensional description of the dynamics. In the present case, we chose to define them in terms of an arbitrary constraint on the potential energy: a portion of the nuclear configurations space is identified with a given complex as long as the associated potential energy varies by less than ΔE_{cut}=0.8 eV relative to equilibrium geometry (the bottom of the potential well).

In practice, we apply a first constraint on the nuclear geometries to restrict the portion of the configuration space which is probed. Each intermediate complex is thus first identified by means of a spheroid analytical function centered on the equilibrium geometry:

$$\frac{\left(r_1 - r_{1\mathrm{eq}}\right)^2}{\Delta r_1^2} + \frac{\left(r_2 - r_{2\mathrm{eq}}\right)^2}{\Delta r_2^2} + \frac{\left(\alpha - \alpha_{\mathrm{eq}}\right)^2}{\Delta \alpha^2} \leq 1 \tag{4}$$

where (r_1,r_2,α) are the relevant internal coordinates, i.e., the bond lengths and the valence bending angle. If the potential wells were fully harmonic, the ranges of geometries Δr_i and $\Delta\alpha$ could have been chosen such as to match exactly the energy criterion ΔE_{cut}. Nevertheless, they are both highly anharmonic, and we thus chose Δq ($q = r_i$ or α) as the maximal value of $|q_{\mathrm{min}} - q_{\mathrm{eq}}|$ and $|q_{\mathrm{max}} - q_{\mathrm{eq}}|$, ($q_{\mathrm{min}}$, q_{max}) being the bond lengths or bending angles which fullfill the energy criterion ΔE_{cut}. For the SiOH intermediate complex, this leads to Δr_{SiO}=0.8 a_0, Δr_{OH}=0.6 a_0, and $\Delta\alpha_{\angle\mathrm{SiOH}}$=52°. For HSiO, we obtain Δr_{SiO}=0.4 a_0, Δr_{SiH}=1.2 a_0, and $\Delta\alpha_{\angle\mathrm{HSiO}}$=51°. In the specific case of SiOH, we wish to emphasize that $\Delta\alpha_{\angle\mathrm{SiOH}}$ has been limited such as the nuclear geometries allocated to the complex do not coincide with the linear saddle point TS2. Once the range of nuclear configurations has been roughly defined by means of Eq. 4, the energy criterion ΔE_{cut} is applied to define more precisely the region allocated to the intermediate complex.

Figure 2 displays the proportion of reactive trajectories involving only SiOH or both complexes as a function of the collision energy. For collision energies below 0.6 eV, the dominant reaction

pathway involves only the formation of the SiOH complex, while, at higher energies, the reaction pathway involving both the SiOH and HSiO complexes becomes the dominant one. It is worth mentionning that no reactive event occurs via the exclusive formation of the HSiO complex, as the SiOH complex is always formed first from the reactants.

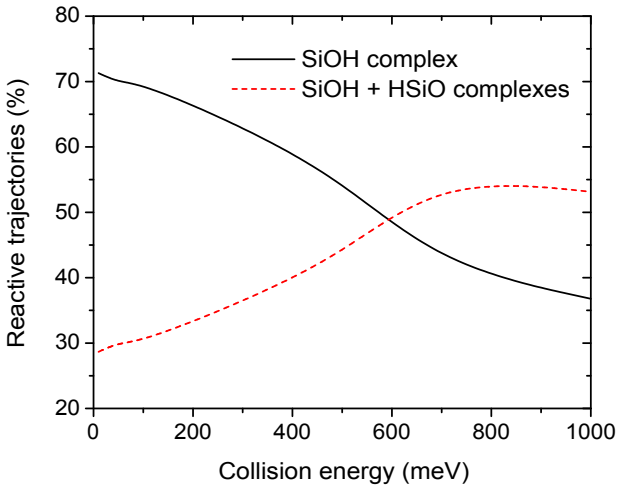

Figure 2: Contributions to the reactivity of the different pathways for the Si+OH(v=0,j=0) → SiO+H reaction

We display in Fig. 3 the average complex lifetimes for the reactive events as a function of collision energy, irrespective of the pathway followed by the system. Following the criterion used in previous works,[15,18,35,36] the intermediate complex is here supposed to be formed when the sum of the three internuclear distances is lower than 6 Å. Its lifetime is defined as the time difference between the first entry and the last exit of the reactive trajectory from this geometrical constraint. A tight complex lifetime is also defined, as the integrated time during which the molecular system fulfills this geometrical constraint. As can be seen, both complex lifetimes increase noticeably with the collision energy. The significant quantitative difference between the two recorded lifetimes stems from trajectories involving large amplitude orbital motion of the incoming Si atom around the OH diatom, resulting from weak intra-vibrational couplings and long range attractive interactions, also known as roaming trajectories.[37,38]

This large amplitude motion, which has already been observed for other triatomic reactions,

e.g. S + OH,[18] N + OH[35] and O + OH,[17] is illustrated in Fig. 4, in which the three interatomic distances, r_{SiO}, r_{OH} and r_{SiH}, are displayed as a function of time for four selected trajectories. These reactive and non-reactive events reveal further details about the mechanisms responsible for the long-lived intermediate complex. Each trajectory corresponds to a collision for which the Si atom initially approaches the O-side of the OH molecule. After the first collision, during which the SiOH complex is temporarily formed, the Si atom is sent back to the reactant channel while a small amount of energy is transferred to the OH rotational motion. The consecutive loss of recoil energy allows the long range potential to bring back the system towards the strong interaction region. The system then experiences multiple quasi-elastic rebounds before back-dissociation (pannel 1 and 3) or reaction (pannel 2 and 4) occur. This dynamics barely affects the OH internuclear distance during a large period of time, thus illustrating the weak coupling between the OH vibrational motion and the translational and orbital motions of Si relative to OH. If the complex does not back-dissociate, the reaction occurs rapidly after the OH vibration of the SiOH intermediate gets sufficiently affected to form HSiO or to dissociate directly into the products SiO+H. The roaming behaviour, which usually reveals non statistical features[37,38] seems to critically depend on the collision energy. The difference between the two above-defined lifetimes, which might be viewed as a rough indicator for roaming, significantly decreases with increasing energy, suggesting an increasing efficiency for IVR. This is concomitant with the increase of the complex lifetime observed in Fig. 3. A similar increase has been previously reported for the S+OH reaction.[18] From pannel 4 of Fig. 4, it can be observed that vibrational couplings between SiO, SiH and OH vibrators appear more important at high energies and take place over a much larger period of time. A rigourous description of roaming dynamics, which requires the accurate study of the phase space geometry,[37,38] is far beyond the scope of the present work.

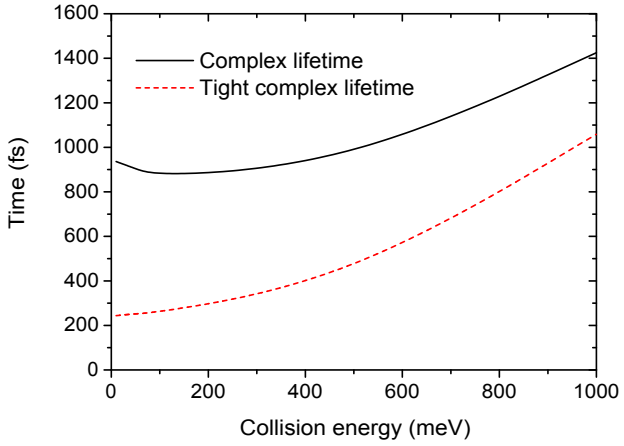

Figure 3: Collision energy dependence of the complex lifetimes for the Si+OH(v=0,j=0) → SiO+H reaction.

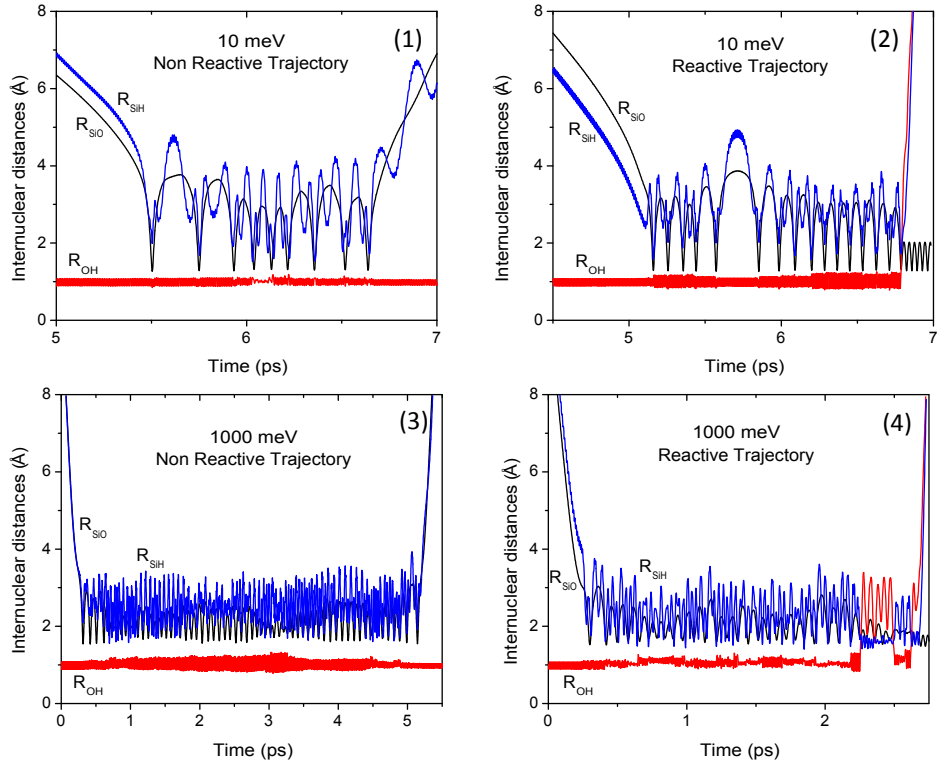

Figure 4: Evolution with time of the interatomic distances r_{SiO} (black), r_{OH} (red) and r_{SiH} (blue) for selected reactive (pannel 2 and 4) and non-reactive (pannel 1 and 3) trajectories at low and high collision energies.

3.2 Reaction probabilities

The reaction probability for the Si+OH(v=0,j=0) → SiO+H reaction is displayed as a function of the collision energy in Fig. 1 of ref.[13] We display in Fig. 5 the reaction probabilities as a function of the impact parameter (opacity functions) at selected collision energies spanning the 10^{-2}-1 eV energy range studied in this work. As can be seen, the reaction probabilities are small and decreasing with increasing energies. This is the consequence of the weak vibrational coupling discussed in the previous section. Back-scattering to the reactants, which involves 50% of collisional events at 10^{-2} eV collision energy, drastically increases up to more than 90 % at 1 eV. This feature is at odd with the expected feature for exoergic and barrierless reactions, governed by the capture of the incoming atom. In such a case, the reaction probability is expected to be close to one up to the maximum impact parameter consistent with complex formation, as it was found for the C+OH reaction.[15] The high efficiency of back-scattering in the cases of the N+OH, O+OH and S+OH reactions was rationalized in terms[16–18] of a phase-space bottleneck inhibiting the intramolecular energy transfer between the O-H and (O,N,S)-O bonds. As highlighted in Fig. 4, the situation is similar here for the coupling between the O-H and Si-O bonds. For the N+OH[16] and O+OH[17] reactions, the opacity functions were found close to step functions up to 0.5 eV collision energy. In the present case, the shape of the opacity function varies significantly with the collision energy, as it was found for the S+OH reaction.[18] For the highest energies, back-scattering is less probable at high impact parameter values for which the initial translational energy is mainly into the orbital motion of the incident atom relative to OH. This evolution with the collision energy suggests a puzzling qualitative change of the back-scattering dynamics. We have not further investigated such a behaviour in the present work.

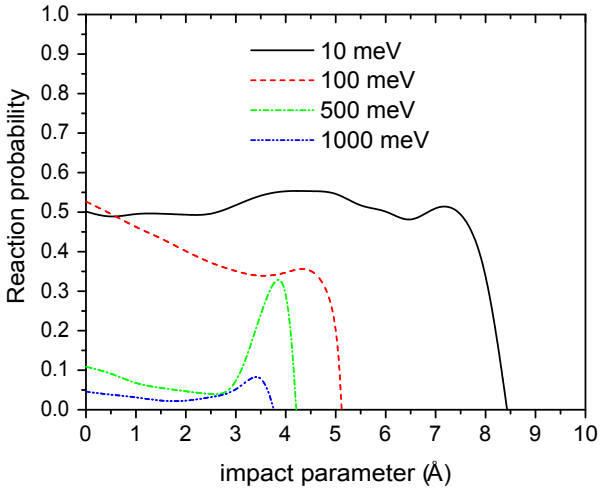

Figure 5: Opacity functions at selected collision energies for the Si+OH(v=0,j=0) → SiO+H reaction.

3.3 Product energy partitioning and differential cross sections

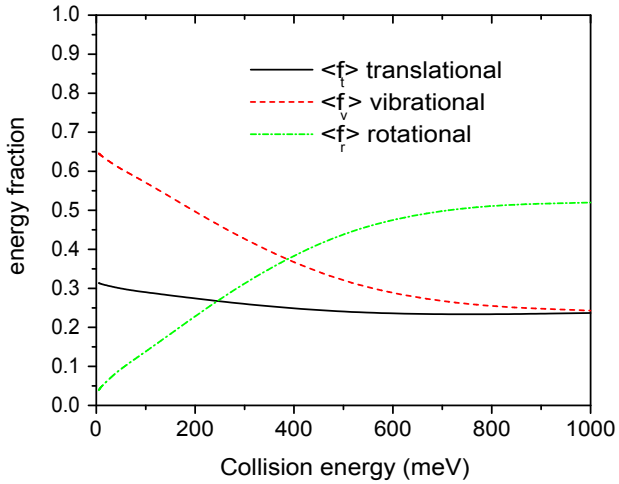

Figure 6: Collision energy dependence of the average fraction of available energy released into the product rotational (green), vibrational (red) and translational (black) modes for the Si+OH(v=0,j=0) → SiO+H reaction.

Figure 6 displays the collision energy dependence of the partition of the available energy released into the vibrational $\langle f_v \rangle$, rotational $\langle f_r \rangle$ and translational $\langle f_t \rangle$ product modes. As can be seen, the fraction of translational energy $\langle f_t \rangle$ remains almost constant, close to 30 %, over the whole collision energy range. This is in contrast with the results obtained for the C+OH,[15] N+OH[35] and

O+OH[17] reactions, for which most of the available energy is channeled into translation in the low energy regime. The energy disposal into the vibrational and rotational modes changes significantly with the collision energy, with a continuous increase of $\langle f_r \rangle$ at the expense of $\langle f_v \rangle$ on increasing the collision energy. Such an increase of the rotational energy disposal with the collision energy has been observed in all the four above mentioned analogous reactions.[15–18] This might be qualitatively understood in terms of kinematic constraints associated with the H + HL → HH + L character of the reaction[39] (H and L stand for heavy and light atoms, respectively). When the reduced mass of the initial fragments is much larger than that of the final ones, the initial orbital angular momentum $|\mathbf{l}|$, which reaches high values at high collision energy, is expected to correlate with the product rotational angular momentum $|\mathbf{j}'|$ due to conservation of the total angular momentum $\mathbf{J}$. As can be seen in Figure 7, while the correlation is poor at low collision energy, it improves noticeably on increasing the collision energy.

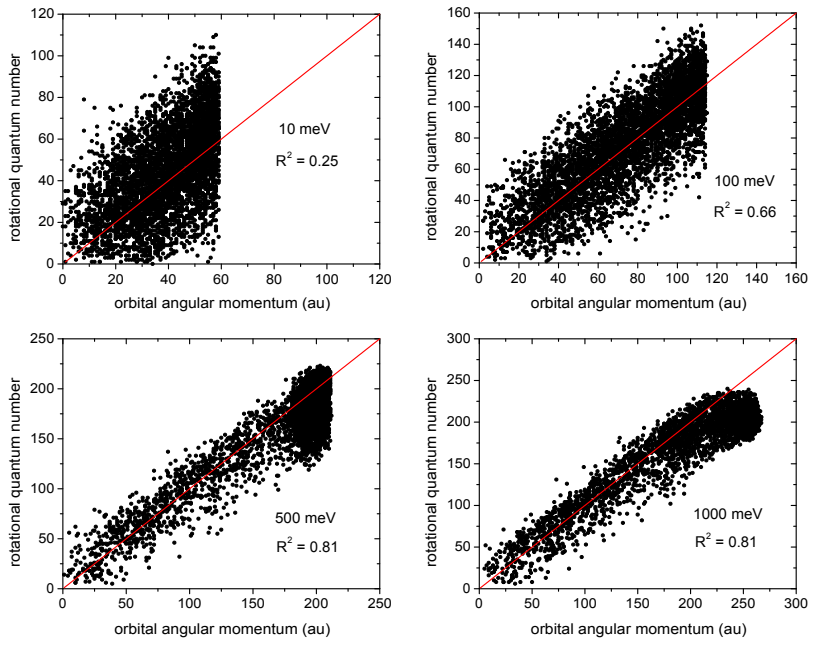

Figure 7: Product rotational quantum number j' as a function of the initial orbital angular momentum l for the Si+OH(v=0,j=0) → SiO+H reaction at selected collision energies.

Figure 8 shows the QCT product translational energy distributions for different collision energies.

The maximum of the translational distribution decreases with the initial collision energy except for E_{coll} = 1000 meV for which the maximum is higher than those obtained for E_{coll} = 100 meV and E_{coll} = 500 meV. In agreement with Figure 6, the product translational energy distributions confirms that the fraction of translational energy transfered to the products after the collision weakly depends on the initial translational energy and that the reaction mechanism, at a given collision energy, is mainly governed by the exchange between vibrational and rotational product modes.

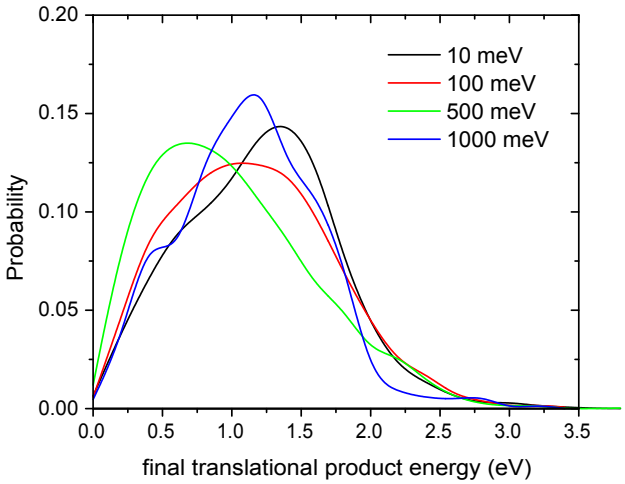

Figure 8: Normalized product translational distribution for the Si+OH(v=0,j=0) → SiO(v')+H reaction at selected collision energies obtained from QCT calculations.

The product vibrational state distributions SiO(v') resulting from QCT and MPPST calculations (MPPST distributions have been normalized to QCT ones) are displayed in Figure 9 for selected collision energies and three different initial rotational states of OH. At low energies (< 0.5 eV) a marked inversion is observed in the QCT results, with a peak close to $v' = 17-20$, in contradiction with statistical predictions. Such a vibrational inversion has also been observed at low collision energy for the S+OH reaction.[18] As the collision energy increases, the lowest vibrational states get more populated and the peak in the product vibrational distribution is shifted toward low v' states, to finally disappear at the highest energy probed. This feature is consistent with the requirement for energy conservation and the kinematic constraints associated with the present H + HL → HH + L reaction. The increase of the SiO rotational excitation with collision energy (see Fig. 6) leads to

a decrease of the amount of energy channelled into the SiO vibrational mode according to energy conservation. Regarding the shape of vibrational state distributions, the comparison between QCT and MPPST results shows that the energy disposal into the SiO vibrational mode evolves gradually from a nonstatistical partition to a statistical one upon increasing collision energy. This feature is consistent with the concommitant increase of the complex lifetime (see Fig. 3). At low collision energies, the dynamics is mainly ruled by a large amplitude motion of the orbiting Si atom, and the reaction occurs rapidly after the OH vibrational motion gets perturbed (see pannel 2 in Fig. 4). In that case, the roaming dynamics seems to be inefficient to randomize the available energy into the complex vibrational modes due to the weak vibrational couplings. At high collision energies, the time that the nuclei remain interacting appears to be large enough for effective energy randomization (see pannel 4 of Fig. 4).

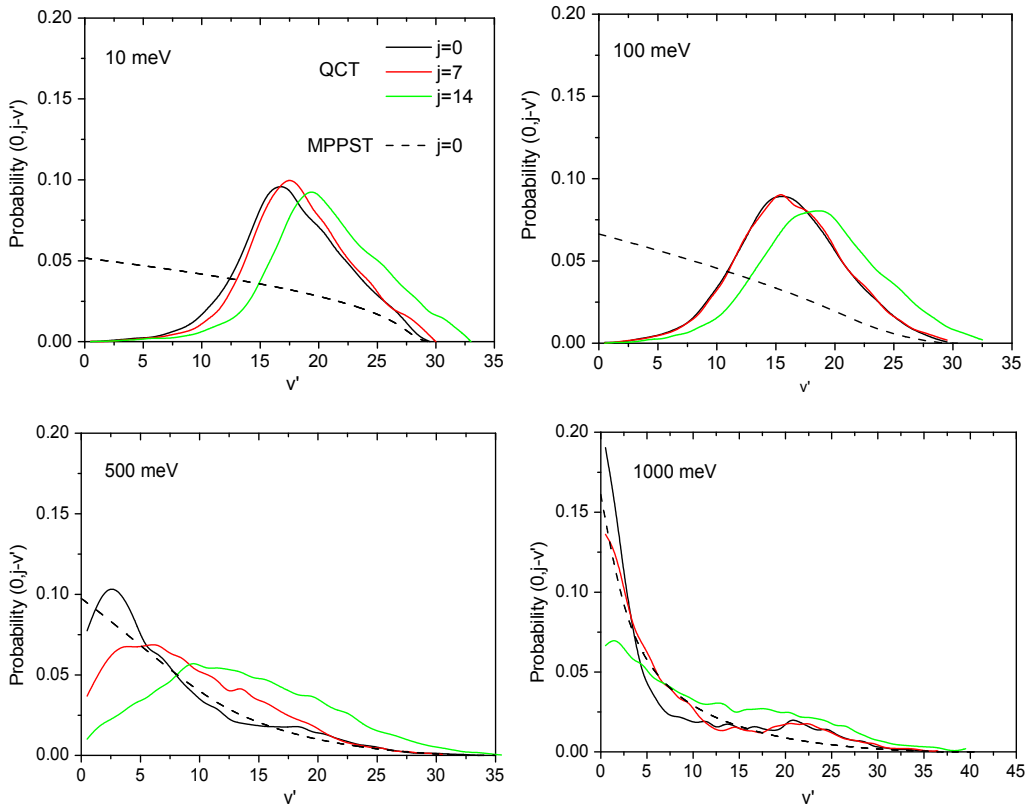

Figure 9: Normalized product vibrational distribution for the Si+OH(v=0, j=0, 7, 14) → SiO(v')+H reaction at selected collision energies obtained from QCT (solid black) and normalized-MPPST (dash black) calculations.

QCT and normalized-MPPST product rotational state distributions SiO(v', j') are displayed in Fig. 10 for the most populated SiO(v') vibrational state at each selected collision energy. As can be seen, the product rotational excitation increases with the collision energy, as predicted from kinematic constraints, and QCT rotational distributions are nicely described by the MPPST results whatever the collision energy range. However, the agreement is somewhat better at low energies than in the high energy range. This is related to the fact that the QCT opacity function largely differs from the step-like functions resulting from statistical calculations. Thus, a correcting factor, taking into account the shape of the opacity function, was introduced in the MPPST treatment, in the spirit of what has been done previously for the O+OH reaction.[17] As can be seen in Fig. 10, such a correction improves the agreement with QCT results at high collision energies. The overall good agreement between the QCT and MPPST product rotational distributions indicates that the SiO rotational mode behaves statistically whatever the collision energy. This feature might be related with the bent structures of the SiOH and HSiO intermediate complexes, which should favor the randomization of energy among rotational degrees-of-freedom.

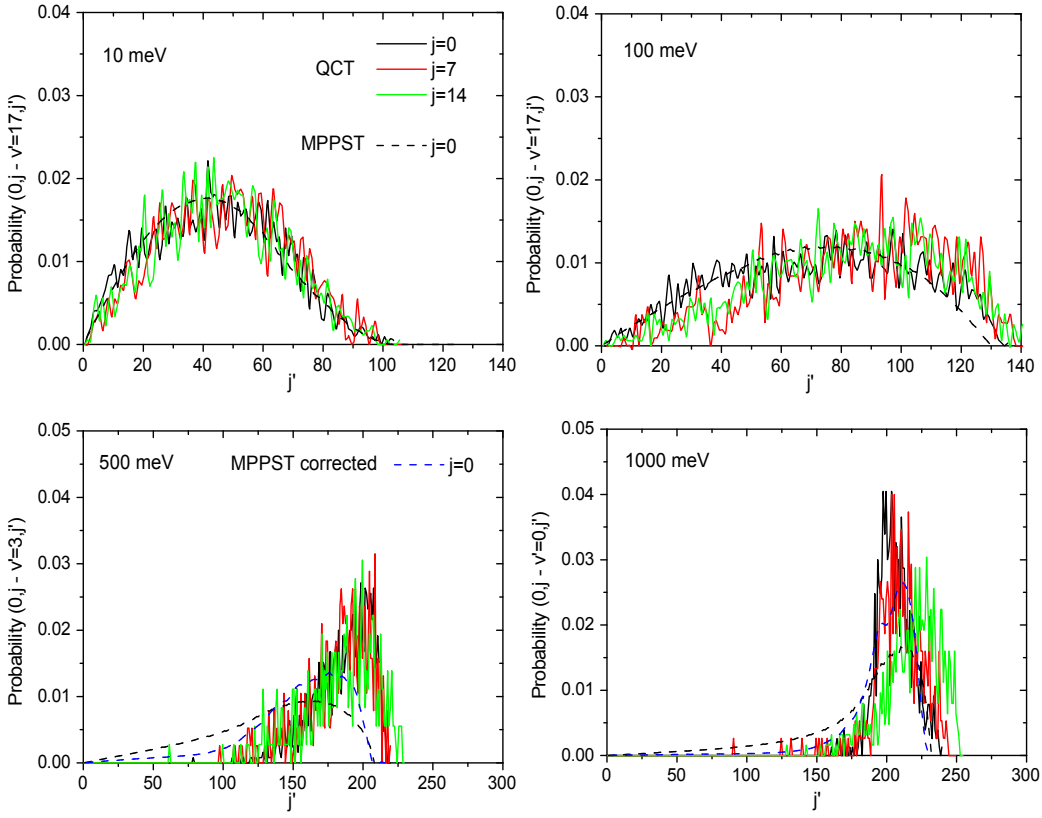

Figure 10: Normalized product rotational distribution for the Si+OH(v=0,j=0, 7, 14) $\rightarrow$ SiO(v',j')+H reaction at selected collision energies obtained from QCT (solid black), normalized-MPPST(dash black) and corrected normalized-MPPST (dash blue) calculations. At each collision energy, the rotational distribution SiO(v', j') for the most populated SiO($v' = 17, 17, 3, 0$) vibrational state is shown.

As can be seen in Fig. 9 and Fig. 10 the initial rotational excitation of the OH molecule has a small influence on the vibrational and rotational distributions. Figure 9 shows that the shape of the vibrational distributions is almost independent of j for $j < 10$ at low collision energies (lower than 200 meV). In contrast, for $j > 10$, distributions are slightly shifted to higher final vibrational states of SiO. At higher collision energies this shift is still observed and a slight enlargement appears. This slight influence of the initial rotation of OH on the dynamics was observed for the reaction probability [13] and shows that the transfert from the rotation to the O-H vibration is favoured when OH is initially highly rotationally excited. The initial rotational excitation of OH marginally affects the rotational product state distributions. Indeed, only a slight shift to larger j' is observed for high energies as can be seen in Fig. 10.

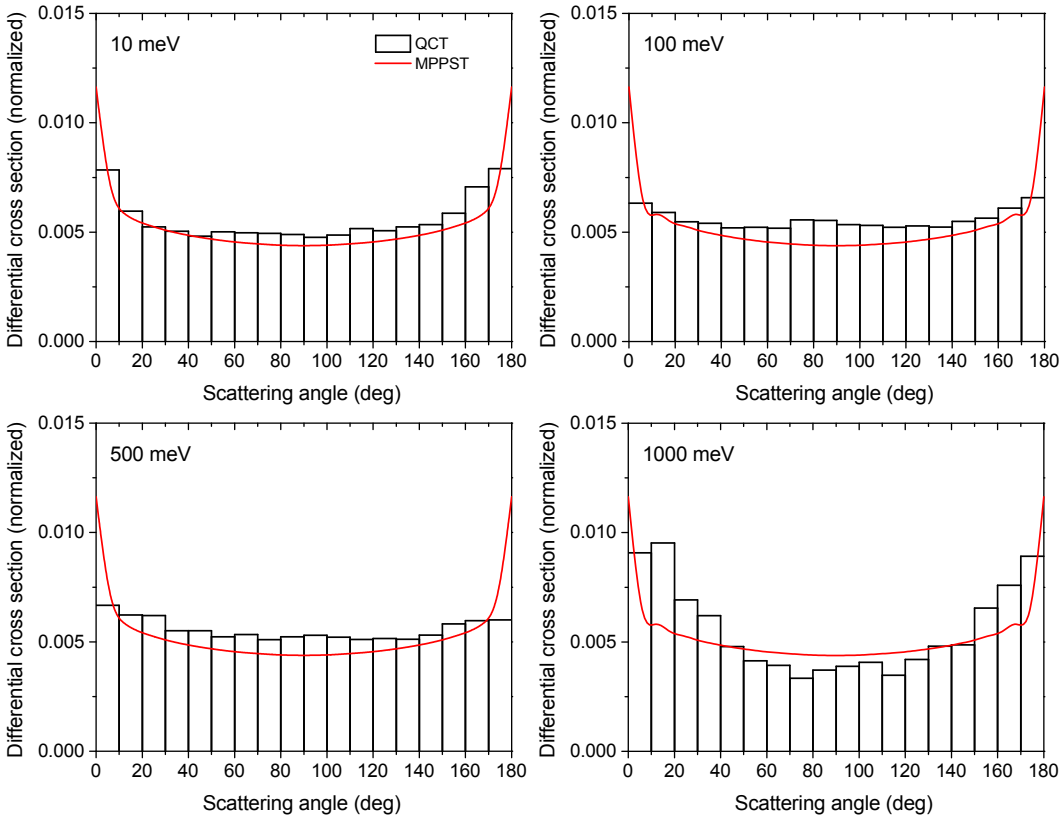

Figure 11: Normalized DCSs for the Si+OH(v=0, j=0) → SiO+H reaction at four collision energies obtained from QCT (black) and MPPST(red) calculations.

Figure 11 shows the total differential cross sections (DCS) for the OH molecule in its initial quantum rovibrational state ($v = 0, j = 0$) at the four collision energies previously considered. Except for the highest one (1000 meV), the agreement between QCT and MPPST DCSs is very good between ~ 10 deg and ~ 170 deg. At the poles, QCT cannot reproduce the MPPST polarization peaks due to parity conservation.[40,41] But ignoring the latter in MPPST calculations would flatten the DCSs at the poles, thus making them in even better agreement with QCT ones. Flat DCSs are typical of H+HL → HH+L reactions behaving statistically.[42–44] Nevertheless, we have seen that at 10 and 100 meV collision energies, the dynamics are clearly nonstatistical as far as the SiO vibrational degree-of-freedom is concerned (see upper pannels in Fig. 9). But one can imagine that the light H atom is so strongly shaken by the heavy SiO diatom in the few tens of femtoseconds previous to its ejection, that the final orbital angular momentum of H with respect to SiO has a random direction, which is just what allows to get a flat DCS. Curiously enough, the

DCS is more polarized at the highest collision energy, i.e., less statistical, in contradiction with the fact that energy distributions are more statistical than in the previous cases. This is an intriguing fact that we plan to analyse in detail in a near future. Finally, no influence of the initial rotational state j of OH on the behavior of DCSs was found, and therefore no results are presented for $j > 0$.

In summary, the comparison of QCT and MPPST product state distributions shows that the bent complex structures is able to couple efficiently the translational and rotational degrees-of-freedom during the complex lifetime whatever the collision energy range. By contrast, the randomization of energy into the vibrational degrees-of-freedom is only effective at the highest collision energies, for which the tight complex lifetime increases noticeably, concomitantly with a decreasing occurence of the roaming mechanism. As a consequence, the reaction dynamics is characterized by a mixed statistical/non-statistical behaviour at low energies, which becomes more statistical at high energies. A similar feature was observed for the S+OH reaction.[18]

4 Conclusions

We have reported a detailed theoretical study of the state-to-state reaction dynamics of the reactive collision Si(^{3}P)+OH($X^2\Pi$) $\rightarrow$ SiO($X^1\Sigma^+$)+H(^{2}S) on the ground X^2A' PES.[10] QCT calculations have allowed to characterize reaction pathways, complex formation dynamics and product state distributions in the 0.01-1 eV collision energy range.

The results show that all collisions proceed through the formation of the SiOH/HSiO intermediate complex, the lifetime of which significantly increases with collision energy. A high probability for back-dissociation to the reactants is found, increasing with increasing collision energy, which can be rationalized in terms of weak couplings between the O-H and Si-O bonds of the SiOH intermediate complex.

The partition of the total available energy into the product modes depends significantly on the collision energy. While the fraction of translational energy remains almost constant, close to 30 %, the rotational energy of the products SiO(v',j') molecules increases rapidly with the collision

energy at the expense of the vibrational energy, consistent with the H + HL → HH + L character of the title reaction. Accordingly, product state distributions and differential cross sections appear to be highly dependent on the collision energy. A marked inversion is observed for the vibrational state distribution at low collision energy, whereas it becomes a motonously decreasing function of v' for increasing collision energy, in agreement with statistical predictions. By contrast, the shapes of rotational state distributions are well reproduced by the results of the statistical approach over the whole energy range.

The reaction is thus governed at low collision energies by a mixed direct/indirect dynamics, mediated by ineffective IVR within the intermediate complex, leading to roaming dynamics in the reactant channel. The resulting product vibrational state distributions are strongly inverted, whereas the translational and rotational degrees of freedom appear efficiently coupled, leading to statistical rotational state distributions. On increasing collision energy, the tight complex lifetime increases, thereby improving IVR, and the product state distributions become consistent with statistical predictions. All these features indicate that the rich and puzzling dynamics of the Si+OH reaction share a lot in common with the previously studied S+OH reaction.[18]

5 Acknowledgments

The Laboratoire de Physique des Lasers, Atomes et Molécules is unité associée au CNRS, UMR 8523. The "Centre d'Étude et de Recherche Lasers et Applications" (CERLA) is supported by the French Ministry of Higher Education and Research, the European Regional Development Fund (ERDF) and the Region "Les Hauts de France". This work was also supported by the Embassy of France in Cuba and the CNRS national program "Physique et Chimie du Milieu Interstellaire".

References

(1) López-Sepulcre, A.; Watanabe, Y.; Sakai, N.; Furuya, R.; Saruwatari, O.; Yamamoto, S. The role of SiO as a tracer of past star-formation events: The case of the high-mass protocluster

NGC 2264-C. Astrophys. J. **2016**, 822, 85.

(2) Widmann, F.; Beuther, H.; Schilke, P.; Stanke, T. SiO: Not the perfect outflow tracer. Astronomy & Astrophysics **2016**, 589, A29.

(3) Martin-Pintado, J.; Bachiller, R.; Fuente, A. SiO emission as a tracer of shocked gas in molecular outflows. Astron. Astrophys. **1992**, 254, 315.

(4) Codella, C.; Bachiller, R.; Reipurth, B. Low and high velocity SiO emission around young stellar objects. Astron. Astrophys. **1999**, 343, 585.

(5) Gusdorf, A.; Cabrit, S.; Flower, D. R.; des Forêts, G. P. SiO line emission from C-type shock waves: interstellar jets and outflows. Astron. Astrophys. **2008**, 482, 809–829.

(6) Langer, W.; Glassgold, A. Silicon chemistry in interstellar clouds. Astrophys. J. **1990**, 352, 123–131.

(7) Schilke, P.; Walmsley, C.; Pineau des Forets, G.; Flower, D. SiO production in interstellar shocks. Astron. Astrophys. **1997**, 321, 293–304.

(8) Le Picard, S.; Canosa, A.; des Forêts, G.; Rebrion-Rowe, C.; Rowe, B. The Si (P)+ O_2 reaction: A fast source of SiO at very low temperature; CRESU measurements and interstellar consequences. Astron. Astrophys. **2001**, 372, 1064–1070.

(9) Casavecchia, P. Chemical reaction dynamics with molecular beams. Rep. Prog. Phys. **2000**, 63, 355.

(10) Dayou, F.; Duflot, D.; Rivero-Santamaría, A.; Monnerville, M. A global ab initio potential energy surface for the X2 A' ground state of the Si + OH → SiO + H reaction. J. Chem. Phys. **2013**, 139, 204305.

(11) Rivero-Santamaría, A. Ab initio, classical, quantum and statistical studies of the Si + OH → SiO + OH reaction. Ph.D. thesis, University of Lille 1 Sciences and Technologies, 2013.

(12) Santamaría, A. R.; Dayou, F.; Rubayo-Soneira, J.; Monnerville, M. Time-Dependent Quantum Wave Packet Study of Si + OH → SiO + H reaction: Cross Sections and Rate Constants. J. Phys. Chem. A **2017**, 121, 1675–1685.

(13) Rivero-Santamaría, A.; Dayou, F.; Rubayo-Soneira, J.; Monnerville, M. Quasi-classical trajectory calculations of cross sections and rate constants for the Si + OH → SiO + H reaction. Chem. Phys. Lett. **2014**, 610–611, 335–340.

(14) Panadés-Barrueta, R.; Rubayo-Soneira, J.; Monnerville, M.; Larregaray, P.; Dayou, F.; Rivero-Santamaría, A. Mean Potential Phase Space Theory Study of the Si + OH → SiO + H reaction. Revista Cubana de Física **2016**, 33.

(15) Zanchet, A.; Halvick, P.; Bussery-Honvault, B.; Honvault, P. Differential cross sections and product energy distributions for the C + OH → CO+ H reaction using a quasiclassical trajectory method. J. Chem. Phys. **2008**, 128, 204301.

(16) Jorfi, M.; Honvault, P.; Halvick, P. Quasi-classical determination of integral cross-sections and rate constants for the N + OH → NO + H reaction. Chem. Phys. Lett. **2009**, 471, 65 – 70.

(17) Jorfi, M.; Honvault, P.; Bargueno, P.; González-Lezana, T.; Larrégaray, P.; Bonnet, L.; Halvick, P. On the statistical behavior of the O + OH → H + O reaction: A comparison between quasiclassical trajectory, quantum scattering, and statistical calculations. J. Chem. Phys. **2009**, 130, 184301.

(18) Jorfi, M.; Honvault, P. Quasi-classical trajectory study of the S + OH → SO + H reaction: from reaction probability to thermal rate constant. Phys. Chem. Chem. Phys. **2011**, 13, 8414–8421.

(19) D. G. Truhlar and J. T. Muckerman, In Atom-molecule collision theory; Bernstein, R. B., Ed.; Plenum, New York, Chapter 16, 1979.

(20) Press, W. H.; Teukolsky, S. A.; Vetterling, V. T.; Flannery, B. P. Numerical Recipes in Fortran, 2nd ed.; Cambridge University Press, Cambridge, 1996.

(21) Miller, W. H. Classical-limit quantum mechanics and the theory of molecular collisions. Adv. Chem. Phys **1974**, 25, 69–177.

(22) Bonnet, L.; Rayez, J.-C. Quasiclassical trajectory method for molecular scattering processes: necessity of a weighted binning approach. Chem. Phys. Lett. **1997**, 277, 183.

(23) Bonnet, L.; Rayez, J.-C. Gaussian weighting in the quasiclassical trajectory method. Chem. Phys. Lett. **2004**, 397, 106 – 109.

(24) Bonnet, L. Classical dynamics of chemical reactions in a quantum spirit. Int. Rev. Phys. Chem. **2013**, 32, 171.

(25) Larregaray, P.; Bonnet, L.; Rayez, J.-C. Validity of semi-classical Phase Space Theory for atom-diatom insertion reactions. J. Phys. Chem. A. **2006**, 110, 1552.

(26) Larregaray, P.; Bonnet, L.; Rayez, J.-C. Mean potential phase space theory of chemical reactions. J. Chem. Phys. **2007**, 127, 084308.

(27) Light, J. C. Phase-Space Theory of Chemical Kinetics. J. Chem. Phys. **1964**, 40, 3221–3229.

(28) Pechukas, P. Transition State Theory. Annu. Rev. Phys. Chem. **1981**, 32, 159–177.

(29) Rivero-Santamaría, A.; González-Martínez, M. L.; González-Lezana, T.; Rubayo-Soneira, J.; Bonnet, L.; Larrégaray, P. The O(1D) + H_2 ($X^1\Sigma^+$, *v, j*) → OH($X^2\Pi$, *v', j'*) + H(^{2}S) reaction at low collision energy: when a simple statistical description of the dynamics works. Physical Chemistry Chemical Physics **2011**, 13, 8136.

(30) Bargueno, P.; Gonzalez-Lezana, T.; Larregaray, P.; Bonnet, L.; Rayez, J.-C. Time dependent wave packet and statistical calculations on the H+O2 reaction. Phys. Chem. Chem. Phys. **2007**, 9, 1127–1137.

(31) Dayou, F.; Larrégaray, P.; Bonnet, L.; Rayez, J.; Arenas, P.; González-Lezana, T. A comparative study of the Si+ O → SiO + O reaction dynamics from quasiclassical trajectory and statistical based methods. J. Chem. Phys. **2008**, 128, 174307.

(32) Nunez-Reyez, D.; Hickson, K. M.; Larregaray, P.; Bonnet, L.; Gonzalez-Lezana, T.; Suleimanov, Y. A combined theoretical and experimental investigation of the kinetics and dynamics of the O(1D) + D_2 at low temperature. Phys. Chem. Chem. Phys. **2018**, 20, 4404.

(33) Bussery-Honvault, B.; Dayou, F. Si + OH interaction: long-range multipolar potentials of the eighteen spin- orbit states. J. Phys. Chem. A **2009**, 113, 14961–14968.

(34) Linstrom, P.; W.G. Mallard, E. NIST Chemistry Web-Book. NIST Standard Reference Database Number 69, Na- tional Institute of Standards and Technology, Gaithersburg MD, 20899 **2008**,

(35) Jorfi, M.; Honvault, P.; Halvick, P. Quasiclassical trajectory calculations of differential cross sections and product energy distributions for the N+ OH → NO+ H reaction. J. Chem. Phys. **2009**, 131, 094302.

(36) Jorfi, M.; Honvault, P.; Halvick, P.; Lin, S.; Guo, H. Quasiclassical trajectory scattering calculations for the OH + O → H+ O_2 reaction: Cross sections and rate constants. Chem. Phys. Lett. **2008**, 462, 53–57.

(37) Bowman, J. M.; Houston, P. L. Theories and simulations of roaming. Chem. Soc. Rev. **2017**, 46, 7615–7624.

(38) Mauguière, F. A.; Collins, P.; Kramer, Z. C.; Carpenter, B. K.; Ezra, G. S.; Farantos, S. C.; Wiggins, S. Roaming: A Phase Space Perspective. Annual Review of Physical Chemistry **2017**, 68, 499–524, PMID: 28375689.

(39) Levine, R. D. Molecular Reaction Dynamics; Cambridge University Press, 2005.

(40) Bonnet, L.; Larrégaray, P.; Rayez, J.-C.; Gonzalez-Lezana, T. Parity conservation and polarization of differential cross sections in complex-forming chemical reactions. Phys. Chem. Chem. Phys. **2006**, 8, 3951–3954.

(41) Bonnet, L.; Larrégaray, P.; Rayez, J.-C. On the theory of complex-forming chemical reactions: effect of parity conservation on the polarization of differential cross sections. Phys. Chem. Chem. Phys. **2007**, 9, 3228–3240.

(42) Case, D. A.; Herschbach, D. R. Statistical theory of angular distributions and rotational orientation in chemical reactions. The Journal of Chemical Physics **1976**, 64, 4212–4222.

(43) Kim, S. K.; Herschbach, D. R. Angular momentum disposal in atom exchange reactions. Faraday Discuss. Chem. Soc. **1987**, 84, 159–169.

(44) Bonnet, L.; Rayez, J.-C. On the key factors of angular correlations in complex-forming elementary reactions. Eur. Phys. J. D. **2006**, 38, 65–73.